Mechanistic Implications in the Phosphatase Activity of Mannich-Based Dinuclear Zinc Complexes with Theoretical Modeling

ARTICLE *in* INORGANIC CHEMISTRY · FEBRUARY 2015

Impact Factor: 4.76 · DOI: 10.1021/ic502937a · Source: PubMed

7 AUTHORS, INCLUDING:

Xuepeng Zhang
Sun Yat-Sen University
16 PUBLICATIONS **55** CITATIONS

SEE PROFILE

Debasis Das
University of Calcutta
76 PUBLICATIONS **806** CITATIONS

SEE PROFILE

Inorganic Chemistry

Article

pubs.acs.org/IC

Mechanistic Implications in the Phosphatase Activity of Mannich-Based Dinuclear Zinc Complexes with Theoretical Modeling

Ria Sanyal,[†,#] Xuepeng Zhang,[‡,#] Priyanka Kundu,[†] Tanmay Chattopadhyay,[§] Cunyuan Zhao,*[,‡] Franz A. Mautner,*[,∥] and Debasis Das*[,†]

[†]Department of Chemistry, University of Calcutta, 92 A.P.C. Road, Kolkata 700009, India

[‡]MOE Key Laboratory of Bioinorganic and Synthetic Chemistry, School of Chemistry and Chemical Engineering, Sun Yat-Sen University, Guangzhou 510275, P. R. China

[§]Department of Chemistry, Panchakot Mahavidyalaya, Sarbari, Purulia 723121, India

[∥]Institut fuer Physikalische und Theoretische Chemie, Technische Universitaet Graz, A-8010 Graz, Austria

Supporting Information

ABSTRACT: An "end-off" compartmental ligand has been synthesized by an abnormal Mannich reaction, namely, 2-[bis(2-methoxyethyl)aminomethyl]-4-isopropylphenol yielding three centrosymmetric binuclear μ-phenoxozinc(II) complexes having the molecular formula $[Zn_2(L)_2X_2]$ (**Zn-1**, **Zn-2**, and **Zn-3**), where X = Cl^-, Br^-, and I^-, respectively. X-ray crystallographic analysis shows that the ZnO_3NX chromophores in each molecule form a slightly distorted trigonal-bipyramidal geometry (τ = 0.55−0.68) with an intermetallic distance of 3.068, 3.101, and 3.083 Å (**1**−**3**, respectively). The spectrophotometrical investigation on their phosphatase activity established that all three of them possess significant hydrolytic efficiency. Michaelis−Menten-derived kinetic parameters indicate that the competitiveness of the rate of P−O bond fission employing the phosphomonoester (4-nitrophenyl)phosphate in 97.5% *N*,*N*-dimethylformamide is **3** > **1** > **2** and the k_{cat} value lies in the range 9.47−11.62 s^{-1} at 298 K. Theoretical calculations involving three major active catalyst forms, such as the dimer-cis form (D-Cis), the dimer-trans form (D-Trans), and the monoform (M-1 and M-2), systematically interpret the reaction mechanism wherein the dimer-cis form with the binuclear-bridged hydroxide ion acting as the nucleophile and one water molecule playing a role in stabilizing the leaving group competes as the most favored pathway.

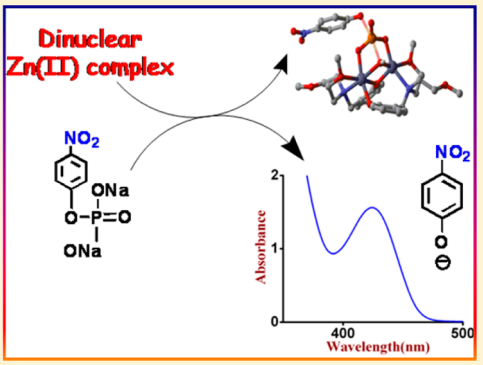

INTRODUCTION

Zinc as a biorelevant metallocatalyst[1] is simply versatile and remarkably efficient in each of its various functional aspects. To elucidate the mysteries in the structure−function interrelationship of a few bimetallic cores and the pros and cons of binuclear metallohydrolases in general and binuclear metallophosphatases in particular at the extremely molecular level, subtle studies with appropriate bioinspired models are on the apex of a pyramid in the research arena.[2−14] Moreover, to identify specific activators and inhibitors as potent components for the synthesis of new drugs and estimate their propensity to act as an efficient metalloenzyme,[15] a paraphernalia of cost-effective but convenient phosphatase assays are essential in fundamental and applied enzymological research.[16] Undeniably, simple metallocomplex-promoted hydrolytic fission of the phosphate bond has been dealt with passionately by organic and inorganic communities alike.[17−24] Ideally, zinc-mediated catalysis is the best in this field and whose versatility in terms of a quintessential metalloenzyme has been proven time and again, which can be primarily attributed to extraordinary ionic potential, leading to high Lewis acidity[25] and coordination flexibility due to closed-shell configuration apart from spontaneous nucleophile generation leaving group stabilization and physiological relevancy. Among them, zinc-containing dinuclear biomimetics are additionally defined[1b,2,26−28] by lower thermodynamic free energy for electron exchange influenced by charge delocalization,[29] a desired orientation of substrates by electrostatic activation, lower activation barrier for solvent and enzyme reorganization, ready formation of hydrolysis-initiating nucleophiles, and stabilized transition states for hydrolysis reactions.[30] Obviously, their rate of reaction is regulated by the mechanistic pathway undertaken, which is as diverse as the possible choices of substrate and complex[1,3d,h,31,32] and the involved catalytic conditions. In a nutshell, the influence of the coordination environment,[33] Zn···Zn distance,[9a] stereochemistry,[3e,8c,d] ligand backbone, and bridger[32,34−36] comprises the family of cardinal determinants, which upon perfect synchronization results in effective catalyst design.

In this study, we have synthesized a new phenolic methoxyethyl pendant "end-off" compartmental Mannich-

Received: December 9, 2014
Published: February 19, 2015

DOI: 10.1021/ic502937a
Inorg. Chem. 2015, 54, 2315−2324

based ligand system, bearing four coordinating sites that yield three 2:2 Zn^{II} complexes. In an epitome, we describe a novel Zn^{II} chemical model as part of our series of studies on the intrinsic chemical properties of Zn^{II} active centers,[33,37,38] whose phosphoester bond cleavage activity has a distinct bifunctional catalytic reaction mechanism (Scheme 1). The possible

Scheme 1. Schematic Depiction of the Hydrolysis Reaction of 4-NPP Catalyzed by Three Symmetrical Mannich-Based Dinuclear Zn^{II} Complexes Differing in the Coordinated Halido Moiety

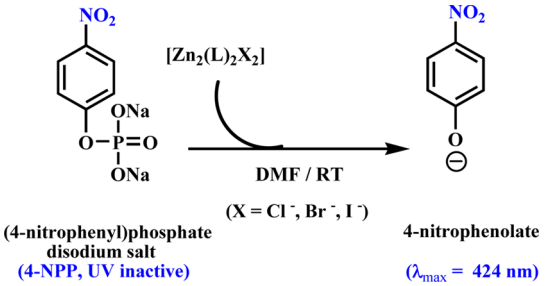

mechanism for (4-nitrophenyl)phosphate (4-NPP) cleavage promoted by **Zn-1**−**Zn-3** is proposed on the basis of kinetic and computational analysis considering six reaction models and 22 reaction pathways. The active catalyst form, determination of the nucleophilic reagent, feasible reaction mechanisms, and participation of solvent molecules during the reaction process are systematically investigated in the calculation. The theoretical results are quite satisfactory, which agrees with our experimental observations and, more importantly, religiously interprets the reaction mechanisms and provides suggestions on the catalyst design. Without any exaggeration, we can comment hereby that not only are our catalysts more robust and less complex than their enzymatic counterpart, they are also blueprints for achieving the dignified rates of "bona fide substrates" with the aid of catalyst design.

EXPERIMENTAL SECTION

Physical Methods and Starting Materials. All of the common organic reagents and solvents used for synthesis were obtained from commercial sources and redistilled before use. *N*,*N*-Dimethylformamide (DMF) was dried according to a literature procedure. The zinc halide salts (AR) were obtained from Merck of anhydrous category. (4-Nitrophenyl)phosphate (4-NPP) was obtained from Sigma-Aldrich. 4-NPP was recrystallized from ethanol/water before use. All other chemicals were of analytical reagant grade. Elemental analyses (carbon, hydrogen, and nitrogen) were performed using a PerkinElmer 240C analyzer. IR spectra (4000−400 cm^{-1}) were recorded at 28 °C on a Shimadzu FTIR-8400S and PerkinElmer Spectrum Express version 1.03 using KBr pellets and NaCl plates as the medium. ^{1}H and ^{13}C NMR spectra (300 MHz) were recorded in $CDCl_3$ and dimethyl sulfoxide (DMSO)-d_6 solvents at 25 °C on a Bruker AV300 Supercon NMR spectrometer. UV−vis spectra and kinetic traces were performed with a Shimadzu 2450 UV−vis spectrophotometer.

Synthesis of the Ligand 2-[Bis(2-methoxyethyl)-aminomethyl]-4-isopropylphenol (HL). To an ethanolic solution (50 mL) of 4-isopropylphenol (25 mmol, 3.4 g) was added dropwise bis(2-methoxyethyl)amine (22.5 mmol, 2.3 g) with constant stirring. After 30 min, a 37% (w/v) formalin solution (22.5 mmol, 1.85 mL) was added to it. The resulting mixture was stirred for 45 min at room temperature and then refluxed for 6 h. It was evaporated under reduced pressure, and the orange oil was extracted with a saturated brine solution and diethyl ether several times. The organic phase was separated, dried with anhydrous $MgSO_4$, concentrated by evaporation of ether, and finally vacuum-dried for removal of the last traces of water. Yield: 4.75 g (75.4%). Elem anal. Calcd for $C_{14}H_{23}N_1O_3$: C, 68.29; H, 9.67; N, 4.98; O, 17.06. Found: C, 68.25; H, 9.69; N, 4.99; O, 17.07. ^{1}H NMR (300 MHz, $CDCl_3$, 25 °C): δ 1.267−1.244 (d, 6H; PhCHCH_3), 2.769−2.806 (t, 4H; NCH_2CH_2), 2.845−2.891 (multiplet, 1H; PhC*H*CH$_3$), 3.323 (s, 6H; OCH_3), 3.530−3.567 (t, 4H; NCH$_2$CH_2), 3.851 (s, 2H; PhCH_2N), 6.714−7.138 (m, 3H; Ar). ^{13}C NMR (300 MHz, DMSO-d_6, 25 °C): δ 24.44 (6H; PhCHCH$_3$), 32.82 (1H; PhCHCH$_3$), 52.86 (2C, OMe), 56.84 (1C, PhCH$_2$N), 58.24 (2C, NCH$_2$CH$_2$), 69.81 (2C, NCH$_2$CH$_2$), 115.43 (1C, Ar), 122.96 (1C, Ar), 125.92 (1C, Ar), 126.95 (1C, Ar), 138.68 (1C, Ar), 155.34 (1C, *Ar*OH). IR data (NaCl plate, cm^{-1}): γ 768, 824, 1017, 1117, 1362, 1256, 1462, 1500, 1596, 1615, 2872.

Table 1. Crystallographic Data and Processing Parameters

	1	2	3
empirical formula	$C_{32}H_{52}Cl_2N_2O_6Zn_2$	$C_{32}H_{52}Br_2N_2O_6Zn_2$	$C_{32}H_{52}I_2N_2O_6Zn_2$
fw	762.44	851.34	945.34
cryst syst	monoclinic	monoclinic	monoclinic
space group	$P2_1/n$	$P2_1/c$	$C2/c$
a, Å	20.858(2)	12.0114(13)	18.8257(18)
b, Å	8.1399(8)	19.4652(19)	12.7316(12)
c, Å	21.673(2)	7.9080(8)	15.8290(16)
α, deg	90.00	90.00	90.00
β, deg	98.09(2)	96.620(17)	99.74(2)
γ, deg	90.00	90.00	90.00
volume, Å^3	3643.1(4)	1836.6(3)	3739.6(7)
Z	4	2	4
μ, mm^{-1}	1.505	3.523	2.975
D_{calc}, Mg m^{-3}	1.390	1.539	1.679
F(000)	1600	872	1888
no. of reflns collected	27944 [R_{int} = 0.0263]	9274 [R_{int} = 0.0285]	14376 [R_{int} = 0.0416]
no. of indep reflns	7393	3677	3800
data/param	7393/405	3677/203	3800/203
GOF	1.041	1.075	1.068
R1 [$I > 2\sigma(I)$]	0.0326	0.0261	0.0325
wR2 (all data)	0.0866	0.0693	0.0816

DOI: 10.1021/ic502937a
Inorg. Chem. 2015, 54, 2315−2324

Synthesis of Zn^{II} Complexes. Synthesis of $[Zn_2L_2Cl_2]$ (Zn-1). A methanolic solution (15 mL) of anhydrous zinc chloride (0.5 mmol, 112.6 mg) was added to a methanolic solution (20 mL) of HL (0.5 mmol, 140 mg). The resulting yellow reaction mixture was allowed to reflux for 2 h. Then the solution was cooled to room temperature, filtered, and kept in a $CaCl_2$ desiccator in the dark. After 1 day, colorless square-shaped crystals, suitable for X-ray data collection, were obtained. Yield: 168 mg (88%). Elem anal. Calcd for $C_{30}H_{48}Cl_2N_2O_6Zn_2$: C, 50.41; H, 6.87; N, 3.67; O, 12.59; Cl, 9.31; Zn, 17.15. Found: C, 50.43; H, 6.81; N, 3.70; O, 12.58; Cl, 9.30; Zn, 17.18. IR data (KBr pellet, cm^{-1}): γ 455, 530, 742, 970, 1020, 1100, 1265, 1492, 1611, 2384, 2954.

Synthesis of $[Zn_2L_2Br_2]$ (Zn-2). Complex **2** was prepared by stirring a solution (20 mL) of ligand (1 mmol, 280 mg) and $ZnBr_2$ (2 mmol, 450 mg) for 30 min. The resulting yellow solution was filtered and kept in a $CaCl_2$ desiccator. A few days later rhombic colorless single crystals were obtained that were suitable for X-ray data collection. Yield: 366 mg (86%). Elem anal. Calcd for $C_{30}H_{48}Br_2N_2O_6Zn_2$: C, 45.14; H, 6.16; N, 3.29; O, 11.28; Br, 18.77; Zn, 15.36. Found: C, 45.15; H, 6.18; N, 3.25; O, 11.29; Br, 18.78; Zn, 15.35. IR data (KBr pellet, cm^{-1}): γ 742, 827, 854, 912, 964, 1022, 1122, 1268, 1490, 1608, 2956.

Synthesis of $[Zn_2L_2I_2]$ (Zn-3). This was prepared by the same procedure as that of complex **2** by using anhydrous zinc iodide (2 mmol, 638 mg) as the metal salt. After 2 days, colorless single crystals appeared from the filtrate when it was kept in room temperature in an yellow oil. It was washed with cold methanol and ether to obtain rectangular good crystals of X-ray crystallographic quality. Yield: 421 mg (89%). Elem anal. Calcd for $C_{30}H_{48}I_2N_2O_6Zn_2$: C, 40.65; H, 5.54; N, 2.96; O, 10.16; I, 26.86; Zn, 13.83. Found: C, 40.64; H, 5.53; N, 2.97; O, 10.19; I, 26.87; Zn, 13.80. IR data (KBr pellet, cm^{-1}): γ 794, 830, 852, 1021, 1116, 1262, 1491, 2959.

X-ray Crystal Structure Analysis. The X-ray single-crystal data of the three compounds were collected on a Bruker-AXS SMART CCD diffractometer at 100(2) K. The crystallographic data, conditions retained for the intensity data collection, and some features of the structure refinements are listed in Table 1. The intensities were collected with Mo Kα radiation (λ = 0.71073 Å). Data processing, Lorentz polarization, and absorption corrections were performed using the *SAINT*, *SMART*, and *SADABS* computer programs.[39] The structures were solved by direct methods and refined by full-matrix least-squares methods on F^2 using the *SHELXTL*[40] program package. All non-H atoms were refined anisotropically. The H atoms were located from difference Fourier maps, assigned with isotropic displacement factors, and included in the final refinement cycles by use of the HFIX utility of the *SHELXTL* program. Molecular plots were performed with the *Mercury* program.[41]

Kinetic Measurements of Hydrolysis of 4-NPP. Disodium (4-nitrophenyl)phosphate hexahydrate was used as the substrate, and the solvent chosen for this study was 97.5% DMF.[33,38] Solutions of substrate 4-NPP and zinc complexes in the solvent were freshly prepared, maintaining the total volume of the reaction mixture at 2 mL. An initial screening of the hydrolytic propensities of all metal complexes was performed until the formation of 2% *p*-nitrophenolate (~2 h) before collection of the kinetic data. The hydrolysis rate of 4-NPP in the presence of complexes **Zn-1**–**Zn-3** was measured by an initial rate method following the absorption increase at 424 nm due to the released 4-nitrophenolate ion in aqueous DMF (ε, 18500 M^{-1} cm^{-1}) at 25 °C. All of the spectra were recorded for 2 h from a solution containing 1 mmol of 4-NPP and 0.05 mmol of the zinc complex. Kinetic experiments were performed at both excess substrate and excess zinc complex, keeping the other conditions constant. Herein we report only the former data. The study comprised five sets having a catalyst of 0.05 mmol and substrate concentrations of 0.5 (10 equiv), 0.7 (14 equiv), 1.0 (20 equiv), 1.2 (24 equiv), and 1.5 mmol (30 equiv). The reactions were initiated by injecting 0.04 mL of metal complex (2.5×10^{-3} M) into 1.96 mL of a 4-NPP solution, and the spectrum was recorded only after complete mixing at 25 °C. The visible absorption increase was recorded for a total period of 30 min at regular intervals of 5 min. All measurements were performed in triplicate, and the average value was assumed. The final A_∞ value for each set was obtained after 2 days (at 25 °C). Finally, the reactions were corrected for the degree of ionization of 4-nitrophenol at 25 °C using the molar extinction coefficients for 4-nitrophenolate at 424 nm.[38b]

Computational Details. The computational work was performed using the *Gaussian 09* program suite.[42] The B3LYP functional[43,44] was utilized for its relatively low computational expense and good data accuracy. Basis sets 6-31G* for C and H atoms, 6-31+G* for O, N, P, and Na atoms, and Lanl2dz for Zn atoms were used for geometry optimization. The single-point energies in the liquid phase were refined by employing diffusion basis sets 6-311++G** for C, H, O, N, P, and Na atoms and Stuttgart/Dresden[45] with an effective core potential for Zn atoms. An empirical dispersion D3 correction was also utilized during the single-point energy refinement in order to well describe the weak interactions. The solvent effect was taken into consideration via the employment of supermolecule calculation (artificially adding several solvent molecules to the reaction complexes) in combination with the single-point polarizable continuum model[46,47] with Truhlar and co-workers' SMD radii (solvent = DMF; E_{ps} = 37.22).[48] Frequency analysis was utilized to distinguish the transition state structures from reaction minima. The free energies of reaction complexes were refined by zero-point correction. The free energies of some reaction complexes involving one or two extra water molecules were corrected by the equation below, which introduces two factors (f and f', both within 0 to 1) to estimate the entropic contributions of transitional and rotational movements, which are actually partially suppressed by the bulk solvent. The f and f' factors in the paper were chosen to be 0.7 in order to be consistent with the substantial structural changes along the reaction coordinates due to the intrinsic high flexibilities of the reaction complexes. This kind of free-energy correction is similar to the method used by Sakaki, Brown, and co-workers.[49] All of the thermodynamic data were obtained at 298.15 K.

$$\Delta G_{corr} = \Delta H - T(\Delta S_{elec} + \Delta S_{vib} + f\Delta S_{trans} + f'\Delta S_{rot})$$

RESULTS AND DISCUSSION

Syntheses and Characterization of Compounds. The Mannich-base "end-off" compartmental ligand used in the present work has been synthesized by the half-Mannich reaction. In this synthetic route, we can selectively isolate the monocondensation product, distinct from the conventional Mannich ligand, which was reported earlier by our group, as the first case of anamolous Mannich synthesis.[33] Likewise, ether extraction and column chromatographic separation yielded the ligand in pure form. It is a tetradentate ligand that resulted in three dinuclear complexes, $[Zn_2(L)_2X_2]$, of 2:2 stoichiometry with anhydrous zinc(II) halide salts having X = Cl^-, Br^-, and I^- (Scheme 2), where the X groups are in the trans orientation.

The ligands and complexes have been completely characterized by standard physicochemical techniques, namely, elemental analysis, Fourier transform infrared (FTIR), ^1H NMR, and UV–vis spectroscopy, and the structure of the Zn^{II} complexes have been further confirmed by single-crystal X-ray diffraction. The FTIR spectra of the ligand and three Zn^{II} complexes show a prominent peak at around 1100 cm^{-1} for the C–N bond stretch and benzene skeletal vibration at around 1490 cm^{-1} (Figures S1–S4 in the Supporting Information, SI). Their NMR and electronic spectra show that they are quite stable in solution, even in highly coordinating solvents like DMF and DMSO (Figures S5–S6 in the SI). Here it may be worth mentioning that we did not provide NMR spectra of the Zn^{II} complexes because they did not show much difference from the ligand NMR because of negligible change in the magnetic environment for coordination to metal ion. Moreover,

DOI: 10.1021/ic502937a
Inorg. Chem. 2015, 54, 2315–2324

Scheme 2. Chemical Drawing of Ligand HL (A) and Complexes Synthesized in the Present Work (B), Where X = Cl^- (Zn-1), Br^- (Zn-2), and I^- (Zn-3)

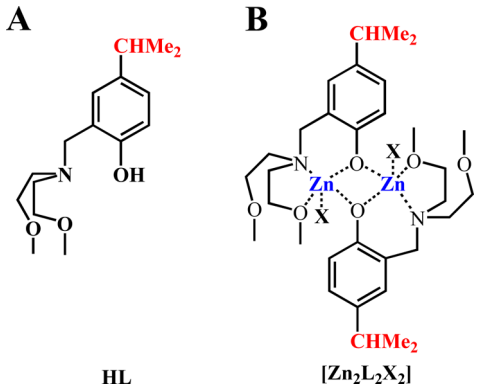

to investigate their electrolytic behavior in a DMF medium, we looked at the molar conductance values of the three complexes, which indicated that they were nonelectrolytes.

The absorption spectra of the ligand in DMF (Figure S7 in the SI) show a lower intense band at ~371 nm probably due to the zwitterionic form of the ligand. Along with it, one higher-energy band of high intensity is observed around 291 nm, which is attributed to the intraligand charge transfer of the open and closed forms of hydrogen-bonded species.[33] The Zn^{II} complexes in its crystalline form display one Soret band at around 280 nm due to the ligand-to-metal-charge-transfer transition and another Q band at roughly 365 nm. Now, in a DMF solution, they exhibit three absorption bands in the regions 230, 285, and 330 nm, out of which the band around 285 nm is of highest intensity. The origin of the two higher-energy peaks may be attributed to the intraligand charge-transfer transition (230−285 nm) and that of the lower-energy band to the ligand-to-metal charge-transfer transition (330 nm), which is composed of a $PhO^- \rightarrow Zn^{II}$ transition or a mixture of the former and $X^- \rightarrow Zn^{II}$.[33,50] The electronic spectra are represented in Figure 1, and all of the UV bands and their molar extinction coefficients are tabulated in a list in Table S1 in the SI.

Description of the Crystal Structures of 1−3. Perspective views together with the partial atom numbering schemes for complexes **1**−**3** are given in Figures 2−4, respectively. The dinuclear complex **Zn-1** of **1** is located on the general positions, whereas the dinuclear complexes $[Zn_2L_2X_2]$ with X = Br (for **2**) and X = I (for **3**) have

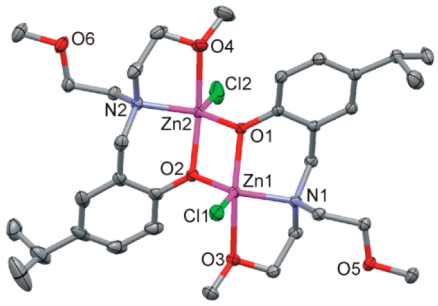

Figure 2. Molecular structure of dinuclear complex **1**. ORTEP drawing with 50% probability ellipsoids. H atoms are omitted for clarity. Selected bond lengths [Å] and angles [deg]: Zn1−O2 1.9597(14), Zn1−O1 2.0601(13), Zn1−N1 2.0880(16), Zn1−O3 2.3499(15), Zn1−Cl1 2.2141(6), Zn1···Zn2 3.0683(6), Zn2−O1 1.9672(13), Zn2−O2 2.0506(14), Zn2−N2 2.0947(17), Zn2−O4 2.3083(16), Zn2−Cl2 2.2205(6); O1−Zn1−O3 161.13(6), N1−Zn1−O2 120.49(6), O1−Zn1−O2 80.45(6), Zn1−O1−Zn2 99.23(6), O1−Zn2−O2 80.51(6), Zn1−O2−Zn2 99.81(6), O2−Zn2−O4 160.76(6), N2−Zn2−O1 121.87(6).

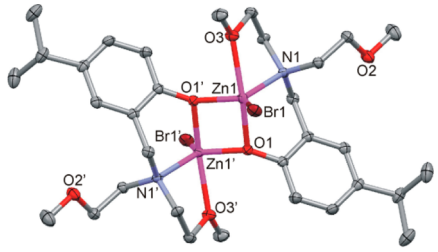

Figure 3. Molecular structure of dinuclear complex **2**. ORTEP drawing with 50% probability ellipsoids. H atoms are omitted for clarity. Selected bond lengths [Å] and angles [deg]: Zn1−O1′ 1.9748(13), Zn1−O1 2.0570(13), Zn1−N1 2.1022(17), Zn1−O3 2.2634(14), Zn1−Br1 2.3587(3), Zn1···Zn1′ 3.1010(5); O1−Zn1−O3 161.05(5), O1′−Zn1−Br1 128.12(4), O1−Zn1−O1′ 79.47(6), Zn1−O1−Zn1′ 100.53(6). Symmetry code (prime): 1 − *x*, −*y*, −*z*.

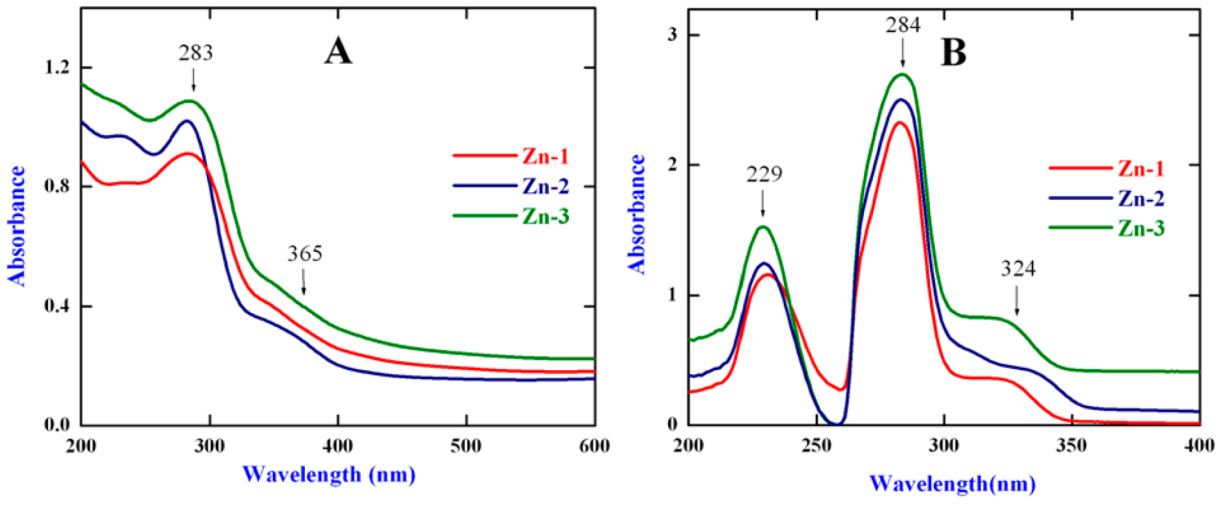

Figure 1. Electronic spectra of the Zn^{II} complexes in (A) the solid state and (B) a DMF solution of concentration 10^{-4} M.

DOI: 10.1021/ic502937a
Inorg. Chem. 2015, 54, 2315−2324

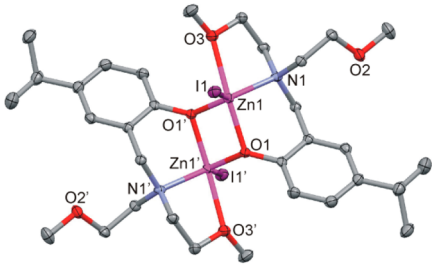

Figure 4. Molecular structure of dinuclear complex **3**. ORTEP drawing with 50% probability ellipsoids. H atoms are omitted for clarity. Selected bond lengths [Å] and angles [deg]: Zn1−O1′ 1.976(2), Zn1−O1 2.069(2), Zn1−N1 2.100(2), Zn1−O3 2.363(2), Zn1−I1 2.5538(6), Zn1···Zn1′ 3.0829(7); O1−Zn1−O3 160.64(8), O1′−Zn1−I1 122.95(6), O1−Zn1−O1′ 80.70(9), Zn1−O1−Zn1′ 99.30(9). Symmetry code (prime): $-x$, $2-y$, $2-z$.

inversion centers. Each Zn^{II} is five-coordinated by two $\mu_{O,O}$-bridging phenoxo O atoms, one N-donor atom of the amine group, one O atom of the two methoxy groups of ligand anion L, and one terminal halide anion. The ZnO_3NX chromophores may be described as distorted trigonal bipyramidal (TBP), and their Addison parameter τ is 0.68 and 0.65 for **1**, 0.55 for **2**, and 0.63 for **3**, respectively (τ = 1 and 0 for ideal trigonal-bipyramidal and square-pyramidal environments, respectively).[51] The $\mu_{O,O}$-bridging phenoxo O atoms are located alternatively in axial and equatorial sites and act as common edges within the dinuclear complexes. The second axial site is occupied by the coordinated methoxo O atom. The axial O−Zn−O bond angles are in the range from 160.64(8) to 161.13(6)°. The Zn−O bond lengths of the bridging phenoxo O atoms vary from 1.9597(14) to 2.069(2) Å, the Zn−N bond distances are in the range from 2.0880(16) to 2.1022(17) Å, and the Zn−O(methoxo) bonds are in the range from 2.2634(14) to 2.363(2) Å, respectively. The terminal halide anions are ligated in the equatorial sites and form Zn−X bond distances of 2.2141(6) and 2.2205(6) Å for **1**, 2.3587(3) Å for **2**, and 2.5538(6) Å for **3**. The Zn···Zn intradimeric separations are 3.0683(6), 3.1010(5), and 3.0829(7) Å for **1**−**3**, respectively. The Zn^{II} centers deviate by 0.095−0.130 Å from their equatorial O−N−X planes.

Phosphatase Activity. To study the phosphatase activity of the zinc complexes, a disodium salt of (4-nitrophenyl)-phosphate hexahydrate was chosen as the substrate. Their hydrolytic tendency was detected spectrophotometrically by monitoring the time evolution of *p*-nitrophenolate (λ_{max} = 424 nm) through a wavelength scan from 200 to 800 nm in aqueous DMF (DMF:water = 97.5:2.5), where the substrate was in 20 equiv of the catalyst, until roughly 2% reaction conversion. The change in the spectral behavior of complex **2** is shown in Figure 5 as a representative scan, and those for the other two are given in the SI (Figures S8 and S9).

Kinetic Studies. The kinetic data, after the Michaelis−Menten treatment, prove that the order of catalytic efficiency is **3** > **1** > **2** in terms of the k_{cat} value, under similar experimental conditions. To elucidate the picturesque, we performed intensive density functional theory (DFT) calculations (Figure 6).

A systematic theoretical modeling utilizing DFT calculations was conducted in order to clarify the active catalyst forms, possible nucleophile, and, more importantly, the plausible reaction mechanisms.

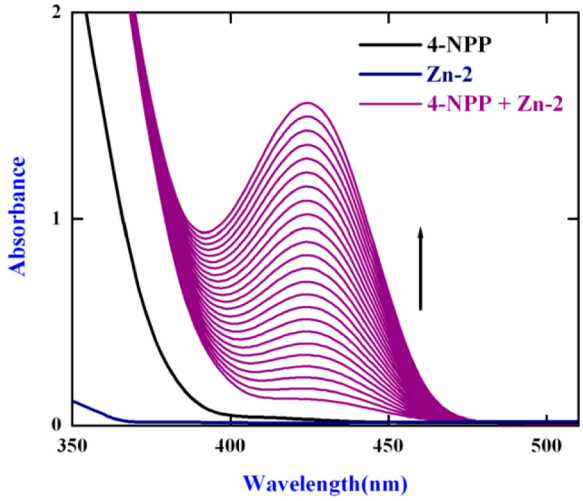

Figure 5. Wavelength scan for hydrolysis of 4-NPP in the absence and presence of complex **Zn-2** (substrate:catalyst = 20:1) in 97.5% DMF recorded at 25 °C at intervals of 5 min. [4-NPP] = 1×10^{-3} M; [complex] = 0.05×10^{-3} M. The arrow shows the change in absorbance with the reaction time.

Theoretical Modeling. The terminal $CHMe_2$ groups were replaced with H atoms in the calculations in order to keep the computational works more tractable for our computational resources. For brevity, L stands for the simplified ligand. The Cartesian coordinates of optimized structures in the proposed mechanisms are provided in the SI (Table S2).

a. Active Catalyst Form. The connections between the symmetrical binuclear μ-phenoxozinc(II) complexes $[Zn_2L_2X_2]$ are two Zn---O coordination linkages, and these noncovalent interactions are not very stable and could be cleaved by the influence of the solvent effects. Therefore, three major active catalyst forms are taken into consideration: the dimer-cis form (D-Cis), the dimer-trans form (D-Trans), and the monoform (M-1 and M-2) (Figure 7). The axial groups in the tetragonal pyramids of the bimetallic center oriented toward the same side in the D-Cis form or toward the opposite side in the D-Trans form. The monoform systems are proven to be less competitive than their dimer counterparts in our calculations, and this is provided in the SI (Figure S10).

b. Reaction Models and Corresponding Reaction Mechanisms. Because of the high flexibilities of the catalyst structures, only the catalyst−substrate binding models of transition states are considered. The hydrolysis mechanism of phosphate monoester dianion NPP^{2-} is generally believed to be a S_N2-type addition−substitution reaction.[52] The nucleophilic reagent could be the metal-bound hydroxide ions or solvent water molecules. The coordination linkages between the substrate NPP^{2-} and the bimetallic centers are various: two Zn---O coordination bonds from the same phosphoryl O atom to the bimetallic center (model 1); two Zn---O bonds to the same Zn^{II} center, with the water molecule acting as the nucleophile (model 3); two Zn---O linkages from two separate phosphoryl O atoms to the bimetallic center (models 4 and 5); three Zn---O coordination linkages between the substrate and the bimetallic center of the catalyst (model 2); the metal-bound hydroxide ion could be axially coordinated (model 4) or bridged (model 5). The proposed reaction models are provided in Figure 8 accompanied by their corresponding reaction transition states in both the D-Cis and D-Trans forms. It is noted that the proposed reaction mechanisms of hydrolysis of

DOI: 10.1021/ic502937a
Inorg. Chem. 2015, 54, 2315−2324

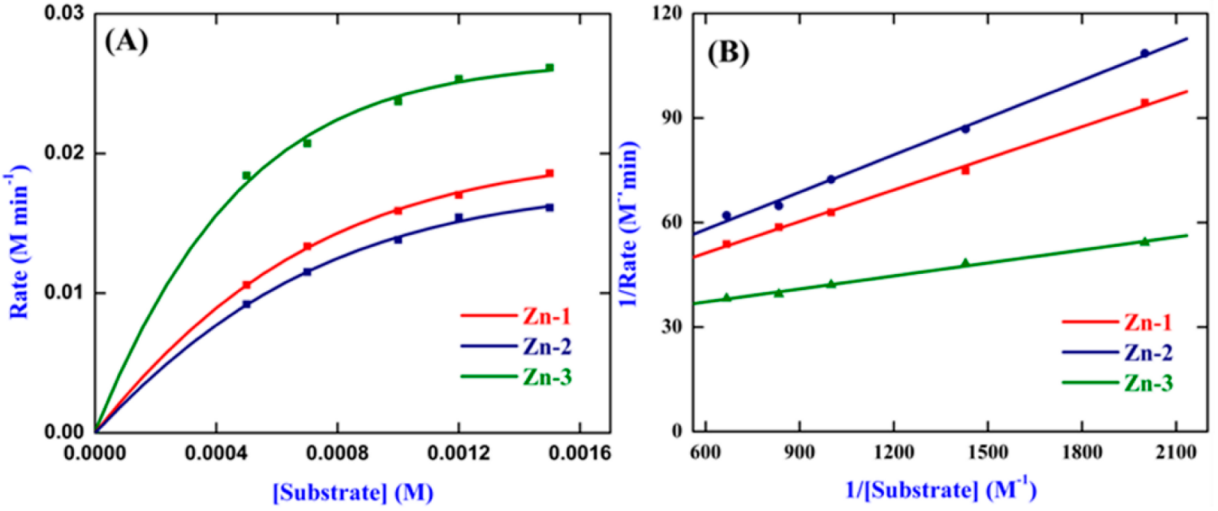

Figure 6. Overlay of the phosphatase activity kinetic plots of the three zinc complexes: (A) enzymatic kinetic plot; (B) Lineweaver–Burk plot.

Table 2. First-Order Rate Parameters for Phosphatase Activity As Obtained by the Michaelis–Menten Treatment of Complexes Zn-1–Zn-3

complex	V_{max} (M s^{-1})	K_m (M)	k_{cat} (s^{-1})
1	0.0005	9.01×10^{-4}	9.97
2	0.00047	1.03×10^{-3}	9.47
3	0.00058	4.59×10^{-4}	11.62

the phosphate monoester dianion NPP^{2-} catalyzed by the dinuclear D-Cis and D-Trans active zinc-containing catalysts are all concerted, which could account for the fact that the planar metaphosphate $[PO_3]^{\ddagger}$ at the equatorial plane of the trigonal-bipyramidal phosphorane in each loose transition state complex is relatively stable and the good leaving group (4-nitrophenyl) at the elongated axis position can be easily dissociated.[52] Besides, potent hydrogen-bonding sites (N–H and O–H sources, etc.) on the second coordination sphere of the bimetallic center are very limited in each active catalyst form, which further enforces the less favorable C–H sites as hydrogen-bond resources to stabilize transition states and possible intermediates (not located). In conclusion, the relatively stable $[PO_3]^{\ddagger}$ plane in each loose transition state in combination with the limited binding sites of the second coordination spheres together result in concerted reaction pathways.

The relative free energies of the above-mentioned transition states are denoted in Figure 9, and by inspection, it could be concluded that the D-Cis form is slightly more catalytically favorable than the D-Trans form. This kind of behavior could be interpreted by the fact that the catalyst–substrate binding complexes are relatively more stable in the D-Cis form, where

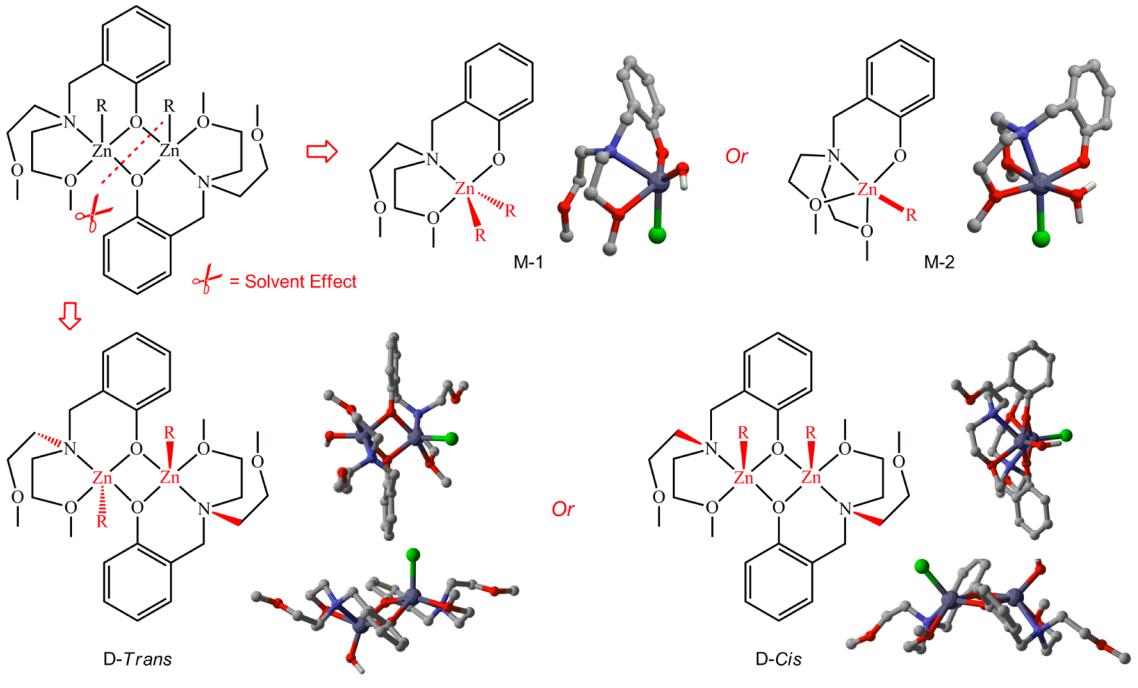

Figure 7. Depicted are the proposed major active catalyst forms.

DOI: 10.1021/ic502937a
Inorg. Chem. 2015, 54, 2315–2324

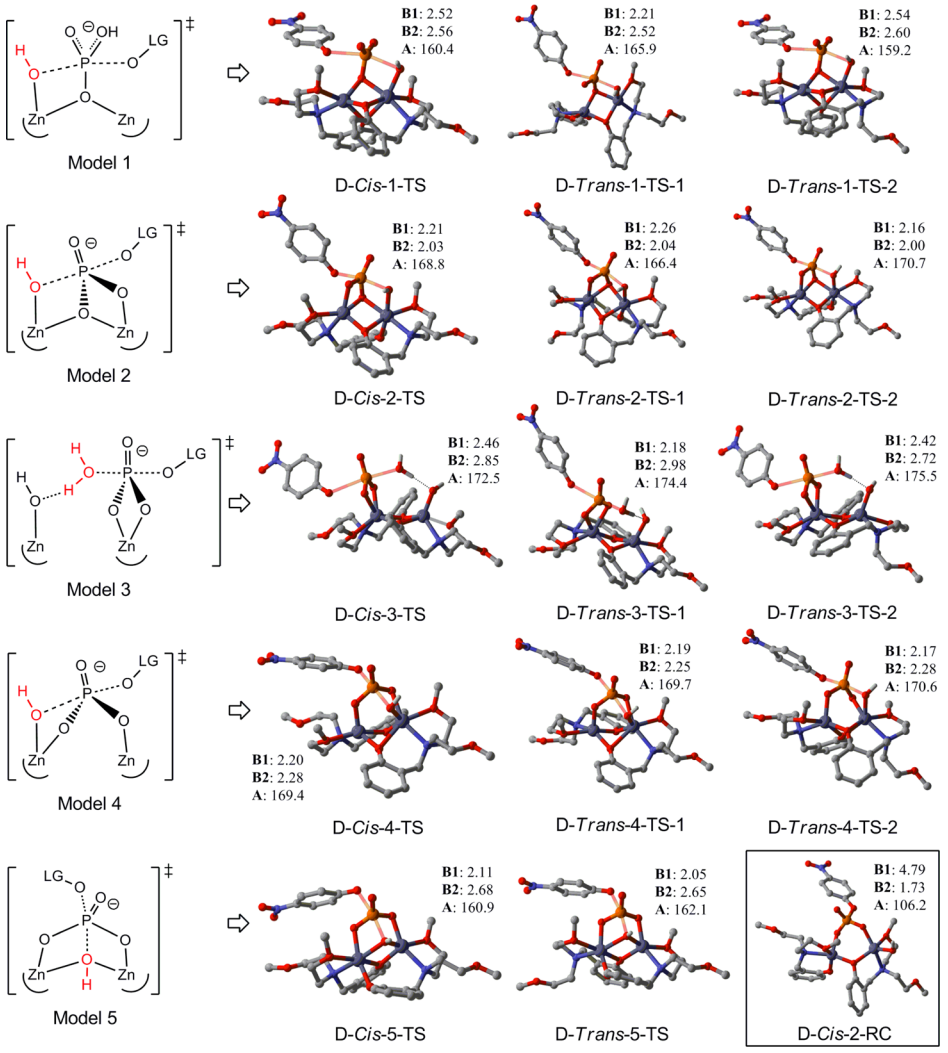

Figure 8. Depicted are the proposed reaction models and their corresponding transition states in both the D-Cis and D-Trans forms. D-Trans-*n*-TS-1 and D-Trans-*n*-TS-2 refer to the transition states in which the axially coordinated OH reagent and its neighboring uncoordinated methoxyethyl side group orient toward the same side or toward opposite sides, respectively. D-Cis-2-RC is the lowest reactant complex. B1 and B2 refer to the bond lengths (in angstroms) of P---O(Nu) and P---O(LG), and A refers to the bond angle (in degrees) of O(Nu)---P---O(LG).

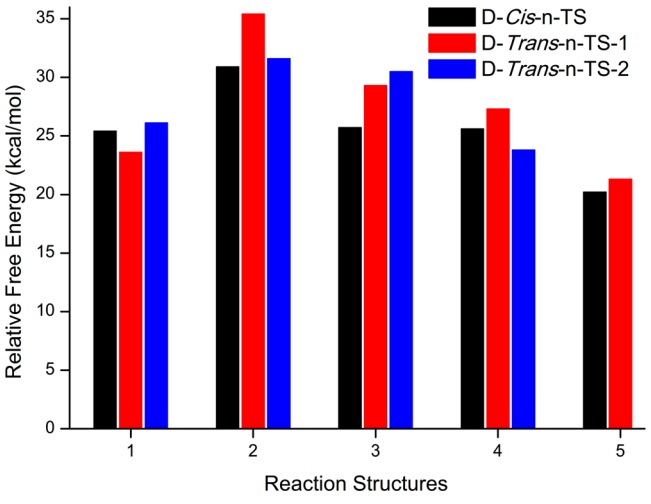

Figure 9. Depicted are the reaction free-energy barriers in the proposed reaction mechanisms utilizing the D-Cis and D-Trans active catalyst forms. The relative free energy of the most stable reactant complex D-Cis-2-RC is set to zero as a reference.

the initially cis-oriented axial coordination sites in the tetragonal pyramids of the bimetallic center could more easily participate in the collaborative stabilization and cleavage of the phosphate monoester substrate. As mentioned above, all of the proposed mechanisms are concerted, and thereby only the PES profiles of the transition state D-Cis-5-TS-involved mechanism are provided (Figure 10).

c. Supermolecule Calculations of the Solvent Effects. Inspection of Figure 9 shows that models 1 and 3 are relatively more catalytically competitive, and, herein, supermolecule calculations operated on the transition states in D-Cis forms in models 1 and 5 were conducted in order to figure out the participation of solvent water molecules and their corresponding effects (as seen in Figure 11).

Inspection of Figure 11 shows that the added water molecules play great roles in the reaction processes: acting as the nucleophile and/or stabilizing the leaving group. The relative free energies of D-Cis-1-$TS_{Wat.-LG}$and D-Cis-1-$TS_{2Wat.-LG}$ are higher than that of D-Cis-1-$TS_{Wat.-Nu.}$, which indicates that the added solvent water molecule(s) is more preferred to act as a nucleophilic reagent than to stabilize the leaving group in model 1. In D-Cis-1-TS, the nucleophile OH-bound Zn^{II} center

DOI: 10.1021/ic502937a
Inorg. Chem. 2015, 54, 2315−2324

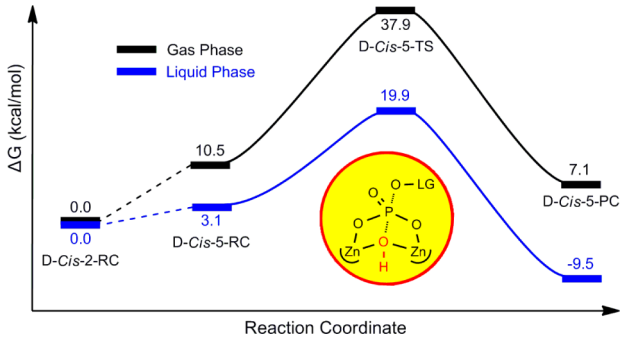

Figure 10. Depicted are the PES profiles of the D-Cis-2-TS-involved reaction mechanism. The relative free energy of D-Cis-2-RC is set to zero as a reference.

is six-coordinated, which was proven to be less stable in our previously reported works.[53] One Zn−O coordination linkage between the two compartmental mononuclear complexes is disconnected when a solvent water molecule is added, and thereby the OH-bound Zn^{II} center is five-coordinated in either D-Cis-1-$TS_{Wat.-Nu.}$ or D-Cis-1-$TS_{Wat.-LG}$, which is commonly believed to be more stable. In model 5, the relative free energy of D-Cis-5-$TS_{Wat.-LG}$ is the lowest among the four transition structures, which is indicative of the fact that the added water molecule is more preferable to stabilize the leaving group than to act as a nucleophile. The mechanistic preferences in models 1 and 5 are different but not contradictory. The space in the compartment nucleophilic attack process is more compact in model 5 than in model 1, which then accounts for the different mechanistic preferences. The bimetallic Zn^{II} centers in model 5 are both five-coordinated, which results in more stable transition states than their counterparts in model 1. In conclusion, model 5, in which the bridged OH acts as the nucleophile, is the most favorable reaction mechanism in both the D-Cis and D-Trans systems. The relative free energy of the most stable transition state D-Cis-5-$TS_{Wat.-LG}$ is estimated to be in the range of 13.2 kcal mol^{-1} ($f = f' = 0.7$, where f and f' are transitional and rotational entropy contribution factors) to 17.3 kcal mol^{-1} ($f = f' = 1$), which is in good agreement with the experimental results (16.1 or 16.0 kcal mol^{-1}, calculated from the observed k_{cat} rate constants reported for the reaction of 9.97 or 11.62 s^{-1}).

d. Catalyst Design. A rational catalyst design study has been conducted by theoretical calculations, as depicted in the SI (Figure S11). The experimental verification of this part has not yet been feasible.

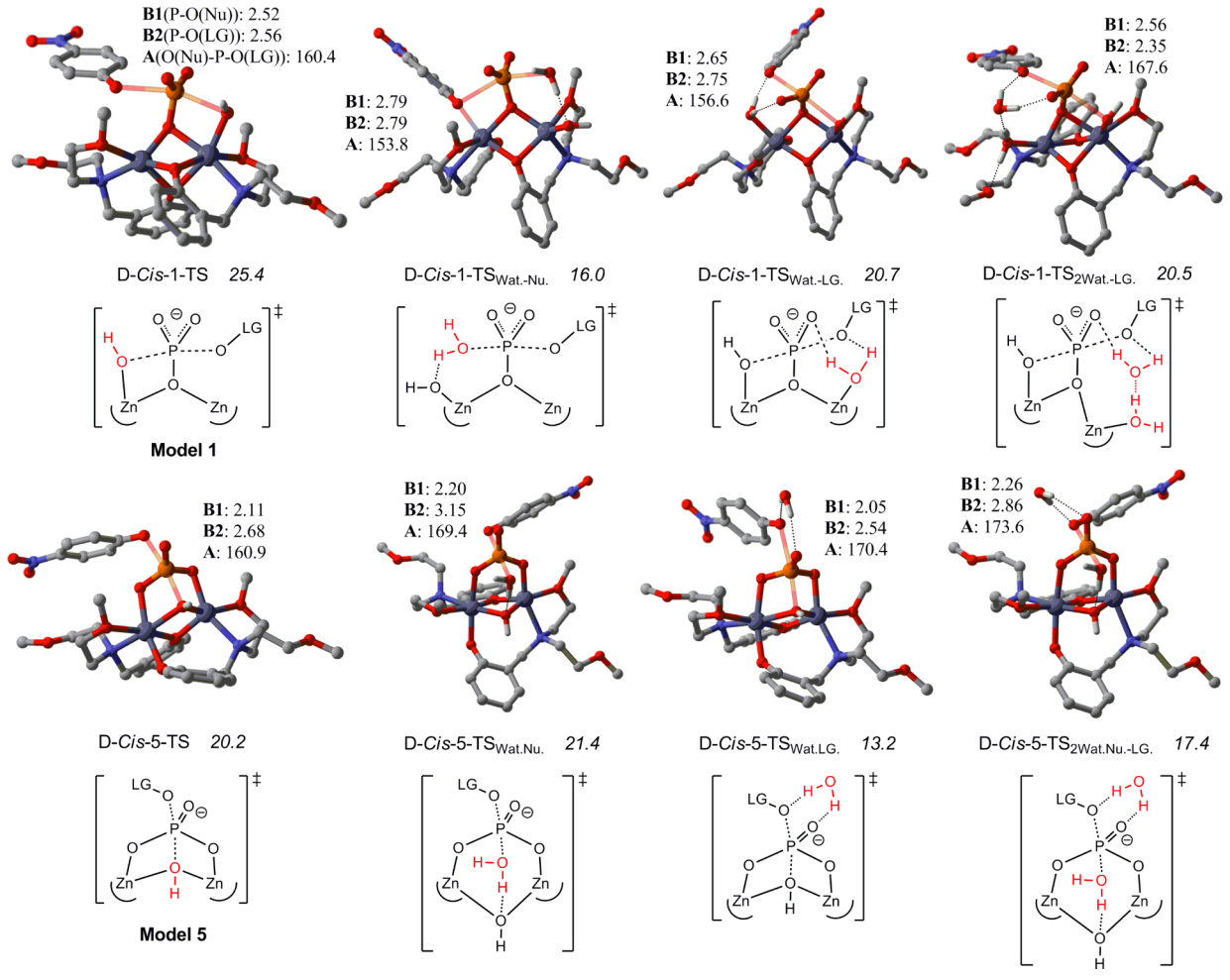

Figure 11. Depicted are the proposed reaction models of the favored models 1 and 5 in combination with the participation of solvent water molecules. The relative free energy of each reaction complex is denoted in italics after the name of corresponding transition structure. B1 and B2 refer to the bond lengths (in angstroms) of P---O(Nu) and P---O(LG), and A refers to the bond angle (in degrees) of O(Nu)---P---O(LG).

DOI: 10.1021/ic502937a
Inorg. Chem. 2015, 54, 2315−2324

CONCLUSIONS

Three synthetic analogues of phosphatase with two zinc centers have been synthesized and characterized. X-ray crystallographic analysis shows that Zn_2L contains a μ-phenoxodizinc(II) core comprised of two quasi-trigonal-bipyramidal zinc complexes that are 3.1 Å apart from each other, being close to the dizinc distance in related natural metalloenzymes. By theoretical modeling, three different kinds of active catalyst forms are discussed, and the D-Cis form, in which the axial coordination sites of the bimetallic center orient toward the same side, is estimated to be catalytically more preferable. Out of five reaction models proposed and optimized, model 5, wherein the bridged OH acts as a nucleophile and two Zn−O coordination linkages are present between the bimetallic center along with two respective terminal phosphoryl O atoms in the transition state, is proven to be the most favorable. The most conventional models 1 and 2 are proven to be less competitive, which might account for the high flexibility of the coordination spheres of the binuclear center. The supermolecule calculation method is utilized to demonstrate participation of the solvent water molecules during the reaction process, and the results show that the added water molecules tend to act as a nucleophile or to stabilize the leaving group. The relative free-energy barrier of the most favorable reaction pathway is in good agreement with the experimental observation. Unfortunately, the influence of a coordinated halide group cannot be theoretically clarified because, first, participation of the halide group during the hydrolysis chemical process of phosphate esters is not reported yet, either in experimental works or through DFT calculations and, second, the difference in the kinetic constants (k_{cat}) in our experimental works is so subtle that it is expediently within the scope of possible experimental errors. Therefore, it seems that participation of the halide group merely happened in a nonchemical phenomenon corresponding to the ligand-exchange processes during the formation of a catalyst−substrate intermediate. It is necessary to mention hereby that the experimental verification of our simulated catalyst design, wherein a benzyl group is utilized to stabilize the leaving group via $\pi-\pi$ stacking interaction, is being dealt with for complete rationalization and extension of this work.

ASSOCIATED CONTENT

Supporting Information

CIF files that provide the crystallographic data for CCDC 1033274, 1033275, and 1033276 for **Zn-1**−**Zn-3**, respectively, listings of FTIR (Figures S1−S4), NMR (Figures S5 and S6), UV−vis (Figure S7 and Table S1), phosphatase activity scans (Figures S8 and S9), competitiveness of the monomer and dimer (Figure S10), catalyst design (Figure S11), and Cartesian coordinates of optimized structures (Table S2). This material is available free of charge via the Internet at http://pubs.acs.org.

AUTHOR INFORMATION

Corresponding Authors

*E-mail: ceszhcy@mail.sysu.edu.cn.
*E-mail: mautner@tugraz.at.
*E-mail: dasdebasis2001@yahoo.com.

Author Contributions

#Equal contribution.

Notes

The authors declare no competing financial interest.

ACKNOWLEDGMENTS

This research is funded by the Council of Scientific and Industrial Research, New Delhi [CSIR Project 01(2464)/11/EMR-II dated 16-05-2011 to D.D.]. R.S. is thankful for a CSIR-SRF fellowship for financial support. F.A.M. thanks Dr. J. Baumgartner (TU-Graz) for assistance and NAWI Graz for support. C.Z. gratefully acknowledges the National Natural Science Foundation of China (Grants 21173273 and 21373277) for financial support. The research is also partially supported by the high-performance grid computing platform of Sun Yat-Sen University, the Guangdong Province Key Laboratory of Computational Science, and the Guangdong Province Computational Science Innovative Research Team.

REFERENCES

(1) (a) Parkin, G. *Chem. Rev.* **2004**, *104*, 699−767. (b) Wilcox, D. E. *Chem. Rev.* **1996**, *96*, 2435−2458.

(2) Mitić, N.; Smith, S. J.; Neves, A.; Guddat, L. W.; Gahan, L. R.; Schenk, G. *Chem. Rev.* **2006**, *106*, 3338−3363.

(3) (a) Kimura, E. *Curr. Opin. Chem. Biol.* **2000**, *4*, 207−213. (b) Morrow, J. R.; Iranzo, O. *Curr. Opin. Chem. Biol.* **2004**, *8*, 192−200. (c) Mancin, F.; Scrimin, P.; Tecilla, P.; Tonellato, U. *Chem. Commun.* **2005**, 2540−2548. (d) Meyer, F. *Eur. J. Inorg. Chem.* **2006**, 3789−3800. (e) Jarenmark, M.; Carlsson, H.; Nordlander, E. *C. R. Chim.* **2007**, *10*, 433−462. (f) Mancin, F.; Tecilla, P. *New J. Chem.* **2007**, *31*, 800−817. (g) Liu, C.; Wang, L. *Dalton Trans.* **2009**, 227−239. (h) Gahan, L. R.; Smith, S. J.; Neves, A.; Schenk, G. *Eur. J. Inorg. Chem.* **2009**, 2745−2758.

(4) Yamaguchi, K.; Akagi, F.; Fujinami, S.; Suzuki, M.; Shionoya, M.; Suzuki, S. *Chem. Commun.* **2001**, 375−376.

(5) (a) Bonfá, L.; Gatos, M.; Mancin, F.; Tecilla, P.; Tonelatto, U. *Inorg. Chem.* **2003**, *42*, 3943−3949. (b) Livieri, M.; Mancin, F.; Saielli, G.; Chin, J.; Tonellato, U. *Chem.—Eur. J.* **2007**, *13*, 2246−2256.

(6) Greatti, A.; Scarpellini, M.; Peralta, R. A.; Casellato, A.; Bortoluzzi, A. J.; Xavier, F. R.; Jovito, R.; de Brito, M. A.; Szpoganicz, B.; Tomkowicz, Z.; Rams, M.; Haase, W.; Neves, A. *Inorg. Chem.* **2008**, *47*, 1107−1119 and references cited therein.

(7) (a) Albedyhl, S.; Averbuch-Pouchot, M. T.; Belle, C.; Krebs, B.; Pierre, J.-L.; Saint-Aman, E.; Torelli, S. *Eur. J. Inorg. Chem.* **2001**, 1457−1464. (b) Albedyhl, S.; Schnieders, D.; Jancsó, A.; Gajda, T.; Krebs, B. *Eur. J. Inorg. Chem.* **2002**, 1400−1409.

(8) (a) Carlsson, H.; Haukka, M.; Nordlander, E. *Inorg. Chem.* **2004**, *43*, 5681−5687. (b) Carlsson, H.; Haukka, M.; Bousseksou, A.; Latour, J.-M.; Nordlander, E. *Inorg. Chem.* **2004**, *43*, 8252−8262. (c) Jarenmark, M.; Kappen, S.; Haukka, M.; Nordlander, E. *Dalton Trans.* **2008**, 993−996. (d) Jarenmark, M.; Csapó, E.; Singh, J.; Wöckel, S.; Farkas, E.; Meyer, F.; Haukka, M.; Nordlander, E. *Dalton Trans.* **2010**, 8183−8194. (e) Jarenmark, M.; Haukka, M.; Demeshko, S.; Tuczek, F.; Zuppiroli, L.; Meyer, F.; Nordlander, E. *Inorg. Chem.* **2011**, *50*, 3866−3887.

(9) (a) Bauer-Siebenlist, B.; Meyer, F.; Farkas, E.; Vidovic, D.; Dechert, S. *Chem.—Eur. J.* **2005**, *11*, 4349−4360. (b) Penkova, L. V.; Maciag, A.; Rybak-Akimova, E. V.; Haukka, M.; Pavlenko, V. A.; Iskenderov, T. S.; Kozłowski, H.; Meyer, F.; Fritsky, I. O. *Inorg. Chem.* **2009**, *48*, 6960−6971.

(10) Selmeczi, K.; Michel, C.; Milet, A.; Gautier-Luneau, I.; Philouze, C.; Pierre, J- L.; Schnieders, D.; Rompel, A.; Belle, C. *Chem.—Eur. J.* **2007**, *13*, 9093−9106.

(11) Belousoff, M. J.; Graham, B.; Spiccia, L. *Eur. J. Inorg. Chem.* **2008**, 4133−4139.

(12) Mohamed, M. F.; Neverov, A. A.; Brown, R. S. *Inorg. Chem.* **2009**, *48*, 11425−11433.

(13) Coleman, F.; Hynes, M. J.; Erxleben, A. *Inorg. Chem.* **2010**, *49*, 6725−6733.

(14) (a) Iranzo, O.; Kovalevsky, A. Y.; Morrow, J. R.; Richard, J. P. *J. Am. Chem. Soc.* **2003**, *125*, 1988−1993. (b) Iranzo, O.; Richard, J. P.; Morrow, J. R. *Inorg. Chem.* **2004**, *43*, 1743−1750.

DOI: 10.1021/ic502937a
Inorg. Chem. 2015, 54, 2315−2324

(15) Von Ahsen, O.; Bömer, U. *ChemBioChem* **2005**, *6*, 481−490.
(16) Sahoo, H.; Hennig, A.; Florea, M.; Roth, D.; Enderle, T.; Nau, W. M. *J. Am. Chem. Soc.* **2007**, *129*, 15927−15934.
(17) Meyer, F.; Pritzkow, H. *Eur. J. Inorg. Chem.* **2005**, 2346−2351.
(18) Albedyhl, S.; Averbuch-Pouchot, M. T.; Belle, C.; Krebs, B.; Pierre, J. L.; Saint-Aman, E.; Torelli, S. *Eur. J. Inorg. Chem.* **2001**, *2001*, 1457−1464.
(19) Belle, C.; Gautier-Luneau, I.; Karmazin, L.; Pierre, J.-L.; Albedyhl, S.; Krebs, B.; Bonin, M. *Eur. J. Inorg. Chem.* **2002**, *2002*, 3087−3090.
(20) Karsten, P.; Neves, A.; Bortoluzzi, A. J.; Lanznaster, M.; Drago, V. *Inorg. Chem.* **2002**, *41*, 4624−4626.
(21) Neves, A.; Lanznaster, M.; Bortoluzzi, A. J.; Perlata, R. A.; Casellato, A.; Castellano, E. E.; Herrald, P.; Riley, M. J.; Schenk, G. *J. Am. Chem. Soc.* **2007**, *129*, 7486−7487.
(22) Batista, S. C.; Neves, A.; Bortoluzzi, A. J.; Vencato, I.; Peralta, R. A.; Szpoganicz, B.; Aires, V. V. E.; Terenzi, H.; Severino, P. C. *Inorg. Chem. Commun.* **2003**, *6*, 1161−1165.
(23) Lanznaster, M.; Neves, A.; Bortoluzzi, A. J.; Szpoganicz, B.; Schwingel, E. *Inorg. Chem.* **2002**, *41*, 5641−5643.
(24) Piovezan, C.; Jovito, R.; Bortoluzzi, A. J.; Terenzi, H.; Fischer, F. L.; Severino, P. C.; Pich, C. T.; Azzolini, G. G.; Peralta, R. A.; Rossi, L. M.; Neves, A. *Inorg. Chem.* **2010**, *49*, 2580−2582.
(25) Ochiai, E.-I. *J. Chem. Educ.* **1988**, *65*, 943−946.
(26) (a) Bazzicalupi, C.; Bencini, A.; Berni, E.; Bianchi, A.; Fornasari, P.; Giorgi, C.; Valtancoli, B. *Inorg. Chem.* **2004**, *43*, 6255−6265. (b) Bazzicalupi, C.; Bencini, A.; Bianchi, A.; Fusi, V.; Giorgi, C.; Paoletti, P.; Valtancoli, B.; Zanchi, D. *Inorg. Chem.* **1997**, *36*, 2784−2790.
(27) Jackson, M. D.; Denu, J. M. *Chem. Rev.* **2001**, *101*, 2313−2140.
(28) Schenk, G.; Mitić, N.; Gahan, L. R.; Ollis, D. L.; McGeary, R. P.; Guddat, L. W. *Acc. Chem. Res.* **2013**, *45*, 1593−1603.
(29) Dismukes, G. C. *Chem. Rev.* **1996**, *96*, 2909−2926.
(30) Daumann, L. J.; Schenk, G.; Ollis, D. L.; Gahan, L. R. *Dalton Trans.* **2014**, *43*, 910−928.
(31) Weston, J. *Chem. Rev.* **2005**, *105*, 2151−2174.
(32) Buchholz, R. R.; Etienne, M. E.; Dorgelo, A.; Mirams, R. E.; Smith, S. J.; Chow, S. Y.; Hanton, L. R.; Jameson, G. B.; Schenk, G.; Gahan, L. R. *Dalton Trans.* **2008**, 6045−6054.
(33) Sanyal, R.; Guha, A.; Ghosh, T.; Mondal, T. K.; Zangrando, E.; Das, D. *Inorg. Chem.* **2014**, *53*, 85−96.
(34) Bazzicalupi, C.; Bencini, A.; Berni, E.; Bianchi, A.; Fornasari, P.; Giorgi, C.; Valtancoli, B. *Inorg. Chem.* **2004**, *43*, 6255−6265.
(35) Bazzicalupi, C.; Bencini, A.; Bianchi, A.; Fusi, V.; Giorgi, C.; Paoletti, P.; Valtancoli, B.; Zanchi, D. *Inorg. Chem.* **1997**, *36*, 2784−2790.
(36) (a) Lippard, S. J.; He, C. *J. Am. Chem. Soc.* **2000**, *122*, 184−185. (b) Xiang, Q.-X.; Zhang, J.; Liu, P.-Y.; Xia, C.-Q.; Zhou, Z.-Y.; Xie, R.-G; Yu, X.-Q. *J. Inorg. Biochem.* **2005**, *99*, 1661−1669. (c) Meyer, F.; Rutsch, P. *Chem. Commun.* **1998**, 1037−1038.
(37) Chakraborty, P.; Adhikary, J.; Sanyal, R.; Khan, A.; Manna, K.; Dey, S.; Zangrando, E.; Bauzá, A.; Frontera, A.; Das, D. *Inorg. Chim. Acta* **2014**, *421*, 364−373.
(38) (a) Kundu, P.; Chakraborty, P.; Adhikary, J.; Chattopadhyay, T.; Fischer, R. C.; Mautner, F. A.; Das, D. *Polyhedron* **2015**, *85*, 320−328. (b) Subat, M.; Woinaroschy, K.; Anthofer, S.; Malterer, B.; Konig, B. *Inorg. Chem.* **2007**, *46*, 4336−4356.
(39) *SAINT*, version 7.23; Bruker AXS Inc.: Madison, WI, 2005. *SMART*; Bruker AXS Inc.: Madison, WI, 2006.
(40) Sheldrick,G. M. *SADABS*, version 2; University of Goettingen: Goettingen, Germany, 2001,
(41) Sheldrick, G. M. *Acta Crystallogr.* **2008**, *A64*, 112−122.
(42) Frisch, G. W. T. M. J.; Schlegel, H. B.; Scuseria, G. E.; Robb, J. R. C. M. A.; Scalmani, G.; Barone, V.; Mennucci, B.; Petersson, H. N. G. A.; Caricato, M.; Li, X.; Hratchian, H. P.; Izmaylov, J. B. A. F.; Zheng, G.; Sonnenberg, J. L.; Hada, M.; Ehara, K. T. M.; Fukuda, R.; Hasegawa, J.; Ishida, M.; Nakajima, T.; Honda, O. K. Y.; Nakai, H.; Vreven, T.; Montgomery, J. A., Jr.; Peralta, F. O. J. E.; Bearpark, M.; Heyd, J. J.; Brothers, E.; Kudin, V. N. S. K. N.; Kobayashi, R.; Normand, J.; Raghavachari, A. R. K.; Burant, J. C.; Iyengar, S. S.; Tomasi, J.; Cossi, N. R. M.; Millam, J. M.; Klene, M. J.; Knox, E.; Cross, J. B.; Bakken, C. A. V.; Jaramillo, J.; Gomperts, R.; Stratmann, R. E.; Yazyev, A. J. A. O.; Cammi, R.; Pomelli, C.; Ochterski, J. W.; Martin, K. M. R. L.; Zakrzewski, V. G.; Voth, G. A.; Salvador, J. J. D. P.; Dapprich, S.; Daniels, A. D.; Farkas, J. B. F. O.; Ortiz, J. V.; Cioslowski, J.; Fox, D. J. *Gaussian 09*; Gaussian, Inc.: Wallingford, CT, 2009.
(43) Becke, A. D. *J. Chem. Phys.* **1993**, *98*, 5648−5652.
(44) Lee, C.; Yang, W.; Parr, R. G. *Phys. Rev. B* **1988**, *37*, 785−789.
(45) Dolg, M.; Wedig, U.; Stoll, H.; Preuss, H. *J. Chem. Phys.* **1987**, *86*, 866−872.
(46) Cossi, M.; Scalmani, G.; Rega, N.; Barone, V. *J. Chem. Phys.* **2002**, *117*, 43−54.
(47) Tomasi, J.; Mennucci, B.; Cammi, R. *Chem. Rev.* **2005**, *105*, 2999−3094.
(48) Marenich, A. V.; Cramer, C. J.; Truhlar, D. G. *J. Phys. Chem. B* **2009**, *113*, 6378−6396.
(49) (a) Sumimoto, M.; Iwane, N.; Takahama, T.; Sakaki, S. *J. Am. Chem. Soc.* **2004**, *126*, 10457. (b) Maxwell, C. I.; Mosey, N. J.; Brown, R. S. *J. Am. Chem. Soc.* **2013**, *135*, 17209.
(50) (a) Annigeri, S. M.; Sathisha, M. P.; Revankar, V. K. *Transition Met. Chem.* **2007**, *32*, 81−87. (b) Annigeri, S. M.; Naik, A. D.; Gangadharmath, U. B.; Revankar, V. K.; Mahale, V. B. *Transition Met. Chem.* **2002**, *27*, 316−320. (c) Naik, A. D.; Revankar, V. K. *Proc. Indian Acad. Sci. (Chem. Sci.)* **2001**, *113*, 285−290.
(51) Addison, A. W.; Rao, T. N.; Reedijk, J.; Rijin, J. V.; Verschoor, G. C. *J. Chem. Soc., Dalton Trans.* **1984**, 1349−1356.
(52) (a) Lipscomb, W. N.; Sträter, N. *Chem. Rev.* **1996**, *96*, 2375−2434. (b) Zhang, X.; Xu, X.; Xu, H.; Zhang, X.; Phillips, D. L.; Zhao, C. *ChemPhysChem* **2014**, *15*, 1887−1898.
(53) (a) Zhang, X.; Zheng, X.; Phillips, D. L.; Zhao, C. *Dalton Trans.* **2014**, *43*, 16289−16299. (b) Zhang, X.; Zhu, Y.; Zheng, X.; Phillips, D. L.; Zhao, C. *Inorg. Chem.* **2014**, *53*, 3354−3361. (c) Zhang, X.; Zhu, Y.; Gao, H.; Zhao, C. *Inorg. Chem.* **2014**, *53*, 11903.

DOI: 10.1021/ic502937a
Inorg. Chem. 2015, 54, 2315−2324